Mathematical Biosciences 262 (2015) 198–205

Contents lists available at ScienceDirect

Mathematical Biosciences

journal homepage: www.elsevier.com/locate/mbs

Mathematical modeling for intracellular transport and binding of HIV-1 Gag proteins

Yuanbin Wang [a,b], Jinying Tan [c], Farrah Sadre-Marandi [d], Jiangguo Liu [d], Xiufen Zou [a,*]

[a] School of Mathematics and Statistics, Wuhan University, Wuhan 430072, China
[b] Department of Mathematics, Shaoxing University, Shaoxing 312000, China
[c] College of Science, Huazhong Agricultural University, Wuhan 430070, China
[d] Department of Mathematics, Colorado State University, Fort Collins, CO 80523, USA

ARTICLE INFO

Article history:
Received 9 July 2014
Revised 12 January 2015
Accepted 14 January 2015
Available online 30 January 2015

Keywords:
Gag protein
HIV-1
Mathematical modeling
Stability
Monomers
Trimers.

ABSTRACT

This paper presents a modeling study for the intracellular trafficking and trimerization of the HIV-1 Gag proteins. A set of differential equations including initial and boundary conditions is used to characterize the transport, diffusion, association and dissociation of Gag monomers and trimers for the time period from the initial production of Gag protein monomers to the initial appearance of immature HIV-1 virions near the cell membrane (the time duration T_a). The existence and stability of the steady-state solution of the initial boundary value problems provide a quantitative characterization of the tendency and equilibrium of Gag protein movement. The numerical simulation results further demonstrate Gag trimerization near the cell membrane. Our calculations of T_a are in good agreement with published experimental data. Sensitivity analysis of T_a to the model parameters indicates that the timing of the initial appearance of HIV-1 virions on the cell membrane is affected by the diffusion and transport processes. These results provide important information and insight into the Gag protein transport and binding and HIV-1 virion formation.

1. Introduction

Human immunodeficiency virus type 1 (HIV-1) is a retrovirus that causes acquired immunodeficiency syndrome (AIDS), a condition in humans in which the immune system progressively fails. The **g**roup specific **a**nti**g**en (Gag) protein plays an important role in the viral life cycle of HIV [1]. The Gag protein is the sole determinant of particle budding, and expression of the Gag protein alone in many eukaryotic cells generates HIV virus-like particles (VLPs) [2]. Therefore, quantitative results for the intracellular trafficking and assembly of Gag proteins are critically important for gaining system-level insights into the process of virus replication and ultimately for developing novel control strategies [3].

In recent years, there have been efforts to develop quantitative models for intracellular transport processes in HIV or other viral infections [4,5]. In [6], intracellular transport is modeled based on molecular motors that pull cargo along a cytoskeletal structure. These molecular cargoes move bidirectionally, involving both the plus and minus directed motors. Studies in [7] concluded that mechanical stochastic tug-of-war models cannot explain this type of bidirectional lipid-droplet transport.

In [8] and [9], interesting results were obtained when the movement of a single virus in cells was simulated using a stochastic model. Other work on quantitative models for intercellular transport were proposed in [10,11]. However, those models mostly focus on the trafficking of a single virus. In [12], all of the species of Gag proteins, including monomers, dimers, and trimers, were treated as quasi-monomers with equivalent concentrations. However, existing biological studies (e.g., [13,15]) revealed that Gag trimers play an important role in binding with the plasma membrane of the infected host cell. Therefore, it is important to develop an integrated mathematical model for the simultaneous treatment of Gag monomers and trimers in the dynamic process of transport and binding.

This paper presents a mathematical model for the characterization of the dynamics of virus trafficking and the transformation between the monomeric and trimeric states by coupling a partial differential equation and an ordinary differential equation (ODE). Based on this model, we find that Gag protein trimers accumulate at the cell membrane. We also estimate when the first new virions would appear near the cell membrane, and our numerical results were in quantitatively good agreement with published experimental results [16].

The rest of this paper is organized as follows. In Section 2, we describe a general model and perform nondimensionalization. In Section 3, we analyze the stability of the steady-state for a special case when there is no diffusion or transport. Section 4 presents the

* Corresponding author. Tel.: +86 2768752958.
E-mail address: xfzou@whu.edu.cn (X. Zou).

http://dx.doi.org/10.1016/j.mbs.2015.01.008
0025-5564/

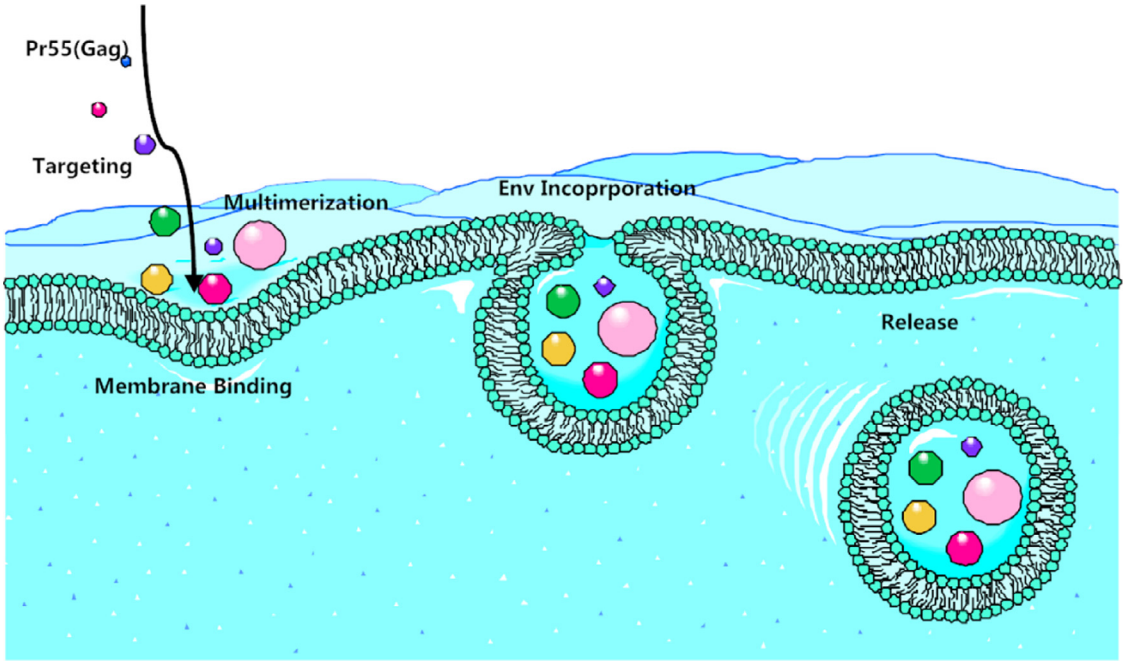

Fig. 1. An illustration of virus assembly process.
Source: [17].

analysis of the steady-state for the general model. In Section 5, numerical simulations are performed to calculate the timing of the initial appearance of new HIV-1 virions on the plasma membrane. The sensitivity analysis of Gag movement to the model parameters is also presented in Section 5. Section 6 concludes the paper with remarks on further work in this research area.

2. A mathematical model and its nondimensionalization

HIV-1 Gag proteins utilize the host cell cytoskeleton for their intracellular movement. HIV-1 particle formation is a multi-step process driven by the viral structural protein Gag [17,18]. Gag protein monomers are produced inside the cytoplasm via the viral mRNA. They egress from the cytoplasm to the cell membrane for further multimerization and assembly. Subsequently, new immature HIV-1 virions bud from the cell membrane, as shown in Fig. 1. Gag proteins can utilize microtubules, dynein and kinesin motor proteins, and the cytoplasm for convection and diffusion. Gag monomers can associate into dimers, trimers, and even higher-order multimers. In turn, the higher-order Gag multimers can dissociate into lower-order multimers as well.

According to [19], Gag proteins often exist in a state of monomer-dimer or monomer-trimer equilibrium. A monomer-trimer association equilibrium exists in the presence of IP6. Under this condition, the concentration of dimeric Gag protein is very low.

Gag monomers do not penetrate back into the cell nucleus, and there is no degradation of Gag monomers. Moreover, due to their size it is reasonable to assume that Gag trimers do not diffuse.

New HIV-1 virions appear and escape their host cells (budding) when the Gag concentration reaches a threshold value. Existing data [20] indicate that approximately 5000 copies of the Gag protein are needed for the assembly of progeny virions. It is reported in [15] that the equilibrium constant K_a is $(4.6 \pm 1.1) \times 10^9\,\mathrm{M}^{-2}$ at temperature 20 °C. This will be used in our numerical simulations.

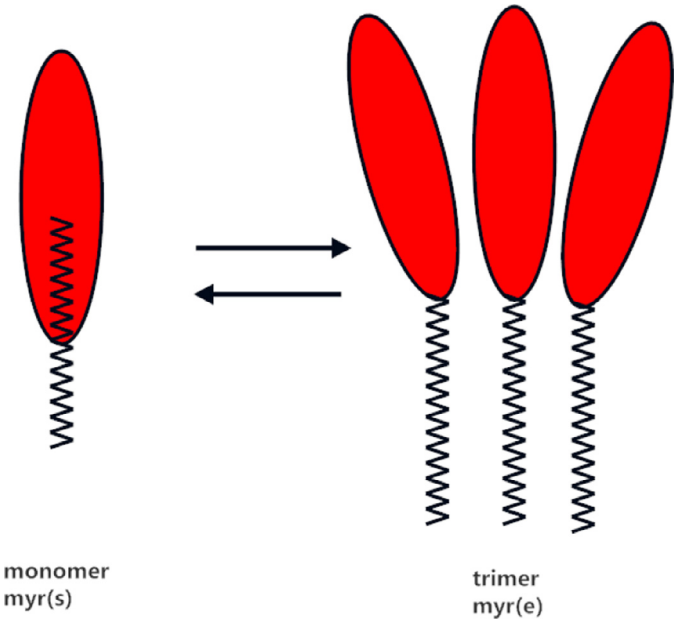

Fig. 2. Transition between monomeric and trimeric states of Gag protein.
Source: [13].

Based on the reported finding in [13] (see Fig. 2), there is a monomer-trimer equilibrium that is described as follows:

$$3\mathrm{Gag}_m \underset{k_{31}}{\overset{k_{13}}{\rightleftharpoons}} \mathrm{Gag}_t, \tag{1}$$

where Gag_m and Gag_t represent the Gag protein monomers and trimers, respectively, and k_{13} and k_{31} represent the two constant reaction rates for monomers associating into trimers and trimers dissociating into monomers, respectively.

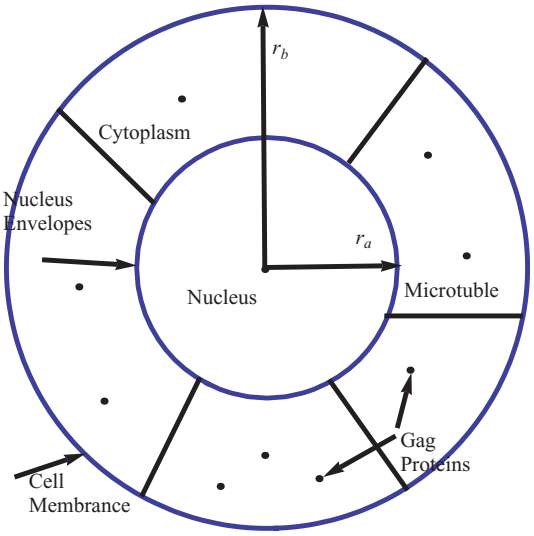

Fig. 3. Annulus as a geometric model for the cytoplasm.

In this study, for the simplicity of modeling we assume that the Gag protein can only exist in the monomeric and trimeric states in the cytoplasm. We also make the following assumptions:

(1) The cytoplasm is modeled by an annulus (Fig. 3);
(2) Gag monomers are produced inside the cytoplasm at a constant rate;
(3) Gag proteins convect and diffuse inside the cytoplasm.

Under these assumptions, we develop a mathematical model using a set of convection-diffusion-reaction equations as follows:

$$\begin{cases} \dfrac{\partial f_1}{\partial t} = \nabla\cdot(D\nabla f_1 - \mathbf{v}f_1) + p_1 - 3k_{13}f_1^3 + 3k_{31}f_3, \\ \quad r\in(r_a,r_b), \quad t>0, \\ \dfrac{\partial f_3}{\partial t} = k_{13}f_1^3 - k_{31}f_3 - \gamma f_3, \quad t>0, \\ \nabla\cdot(D\nabla f_1 - \mathbf{v}f_1)|_{r=r_a} = 0, \quad \nabla\cdot(D\nabla f_1 - \mathbf{v}f_1)|_{r=r_b} = 0, \\ f_1(r,t) = 0, \quad f_3(r,t) = 0, \quad r\in[r_a,r_b], \quad t=0, \end{cases} \tag{2}$$

where $f_1(r,t)$ and $f_3(r,t)$ are the concentrations of the Gag protein monomers and trimers at position r and time point t, D is the Gag monomer diffusion rate, $\mathbf{v}$ is the velocity of the Gag monomers, r_a and r_b are the radii of the nucleus and the plasma membrane, respectively, p_1 is the constant production rate of Gag monomers, and γ is the degradation rate of Gag protein trimers.

The two boundary conditions imply that Gag monomers do not penetrate back into the nucleus and will not escape from the cytoplasm until the Gag protein concentration near the cell membrane reaches a threshold value, allowing new virions to form.

Note that although the Gag proteins can move along the microtubules in both directions, we consider only the transport with an averaged velocity toward the cell membrane. For simplicity, we set the radial direction vector of the microtubules as $\vec{\mathbf{n}}$ and the velocity as $\mathbf{v} = s\vec{\mathbf{n}}$.

We further introduce dimensionless quantities through scalings as follows:

$$\begin{aligned} &\tau = t(k_{31}+\gamma), \quad \delta_1 = \frac{D}{r_b^2(k_{31}+\gamma)}, \quad \delta_2 = \frac{s}{r_b(k_{31}+\gamma)}, \\ &\eta = \frac{r_a}{r_b}, \quad \delta_3 = \frac{k_{13}p_1^2}{(k_{31}+\gamma)^3}, \quad \delta_4 = \frac{k_{31}}{k_{31}+\gamma}, \quad f_1 = \frac{p_1}{k_{31}+\gamma}\phi_1, \\ &f_3 = \frac{p_1}{k_{31}+\gamma}\phi_3, \quad r = r_b\rho, \quad \delta_{21} = \frac{sr_b}{D}. \end{aligned} \tag{3}$$

Substituting the above new variables in (3) into Eq. (2), we obtain the following dimensionless model.

$$\begin{cases} \dfrac{\partial\phi_1}{\partial\tau} = \delta_1\dfrac{\partial^2\phi_1}{\partial\rho^2} + \dfrac{\partial\phi_1}{\partial\rho}\left(\dfrac{\delta_1}{\rho} - \delta_2\right) - \dfrac{\delta_2}{\rho}\phi_1 \\ \qquad\qquad + 1 - 3\delta_3\phi_1^3 + 3\delta_4\phi_3, \quad \rho\in(\eta,1), \quad \tau>0 \\ \dfrac{\partial\phi_3}{\partial\tau} = \delta_3\phi_1^3 - \phi_3, \quad \tau>0 \\ \left(\dfrac{\partial\phi_1}{\partial\rho} - \delta_{21}\phi_1\right) = 0, \quad \text{at} \quad \rho=\eta \text{ or } 1, \\ \phi_1(\rho,\tau) = 0, \quad \phi_3(\rho,\tau) = 0, \quad \rho\in[\eta,1], \quad \tau = 0. \end{cases} \tag{4}$$

For this model, we introduce an equilibrium constant $K_\alpha = \frac{k_{13}}{k_{31}+\gamma}$, so that we can rewrite δ_3 as $\delta_3 = K_\alpha\frac{p_1^2}{(k_{31}+\gamma)^2}$. The dimensionless parameters $\delta_1, \delta_2, \delta_3$ and δ_4 are interpreted as the diffusion ratio, transport ratio, association and degradation efficiency of the trimers, respectively.

3. Analysis of the solutions of a simplified model

In this section we simplify the proposed model by considering a state with no transport and no diffusion of Gag proteins ($\delta_1 = \delta_2 = 0$). The purpose of doing so is to examine the consequences of association and dissociation among Gag monomers and trimers. In this case, Eq. (4) becomes

$$\begin{cases} \dfrac{d\phi_1}{d\tau} = 1 - 3\delta_3\phi_1^3 + 3\delta_4\phi_3, \\ \dfrac{d\phi_3}{d\tau} = \delta_3\phi_1^3 - \phi_3, \\ \phi_1(0) = 0, \quad \phi_3(0) = 0, \quad \tau = 0. \end{cases} \tag{5}$$

Theorem 3.1. *The solutions of IVP (5) are positive and bounded. Furthermore, the steady-state solution of (5) is locally asymptotically stable for $\delta_3 > \delta_4^2$.*

Proof. Let (ϕ_1^*, ϕ_3^*) be the solutions of (5).

First, we prove that the solutions (ϕ_1^*, ϕ_3^*) are positive. Without a loss of generality, we set $\phi_1^*(\tau) = 0, \phi_3^*(\tau) > 0$ at $\tau = \tau_1$. From the 1st ODE in (5), we have $\dfrac{\partial\phi_1^*}{\partial\tau} = 1 + 3\delta_4\phi_3^* > 0$. This means that $\phi_1^*(\tau_1 + \Delta\tau) > 0$. Thus, the solutions of (5) are always positive.

Next, let $B(\tau) = \phi_1^*(\tau) + 3\phi_3^*(\tau)$. We easily see that $B(\tau)$ is always positive because ϕ_1^* and ϕ_3^* are positive. Therefore, there exists a constant γ_0 such that the following holds

$$\gamma_0 B(\tau) < \phi_3^* < \frac{1}{3}B(\tau), \quad 0 < \gamma_0 < \frac{1}{3}. \tag{6}$$

From Eq. (5) and $\delta_4 = \dfrac{k_{31}}{k_{31}+\gamma} < 1$, we have

$$\frac{dB(\tau)}{d\tau} = 1 - 3(1-\delta_4)\phi_3^* < 1 - 3(1-\delta_4)\gamma_0 B(\tau). \tag{7}$$

When τ is large enough, $B(\tau) < \dfrac{1}{3(1-\delta_4)\gamma_0} + 1$ and hence is bounded, which in turn forces ϕ_1^* and ϕ_3^* to be bounded.

Next, we analyze the stability of the steady-state solution of (5). Direct calculations lead to an equilibrium point

$$(\phi_1^T, \phi_3^T) = \left(\sqrt[3]{\frac{1}{3\delta_3(1-\delta_4)}}, \frac{1}{3(1-\delta_4)}\right). \tag{8}$$

Substituting $u = \phi_1 - \phi_1^T$ and $v = \phi_3 - \phi_3^T$ into Eq. (5), after linearization with respect to u and v we have

$$\begin{cases} \dfrac{du}{d\tau} = -9\delta_3 u(\phi_1^T)^2 + 3\delta_4 v, \\ \dfrac{dv}{d\tau} = 3\delta_3 u(\phi_1^\tau)^2 - v. \end{cases} \tag{9}$$

The eigenvalues of the above system are

$$\begin{cases} \lambda_1 = \frac{1}{2}(-A - C), \\ \lambda_2 = \frac{1}{2}(-A + C), \end{cases} \tag{10}$$

where

$$\begin{cases} A = 1 + 3^{4/3}\delta_3^{1/3}(1-\delta_4)^{-2/3}, \\ C = \sqrt{\begin{array}{l} 1 - 2 * 3^{4/3}\delta_3^{1/3}(1-\delta_4)^{-2/3} + 4 * 3^{4/3}\delta_4^2 \\ (\delta_3 - \delta_3\delta_4)^{-2/3} + 3^{8/3}\delta_3^{2/3}(1-\delta_4)^{-4/3} \end{array}}. \end{cases} \tag{11}$$

It is easy to know that λ_1 is negative. Let $L = A^2 - C^2$, we have

$$L = 12 * 3^{1/3}(1-\delta_4)^{-2/3}\delta_3^{2/3}(\delta_3 - \delta_4^2). \tag{12}$$

When $\delta_3 > \delta_4^2$, we have $L > 0$. It is shown that λ_2 is negative. Therefore, the solutions of (5) are asymptotically stable, which concludes the proof.

Remark. The biological implication of Theorem 3.1 is that the concentrations of the monomers and trimers will eventually reach an equilibrium if no active transport or diffusion is present [14].

4. Analysis of the steady-state solution of the general model

This section presents analysis of the steady-state solution of the general model in Eq. (4).

Let $\dfrac{\partial\phi_1}{\partial\tau} = 0$ and $\dfrac{\partial\phi_3}{\partial\tau} = 0$. Then, the dimensionless Eq. (4) is transformed into an ODE as follows

$$\begin{cases} \delta_1\rho\dfrac{\partial^2\phi_1}{\partial\rho^2} + \dfrac{\partial\phi_1}{\partial\rho}(\delta_1 - \delta_2\rho) - 3\delta_3\rho\phi_1^3(1-\delta_4) - \delta_2\phi_1 + \rho = 0, \\ \quad \rho \in (\eta, 1), \\ \dfrac{\partial\phi_1}{\partial\rho} - \delta_{21}\phi_1 = 0, \quad \text{for } \rho = \eta \text{ or } 1. \end{cases} \tag{13}$$

It is difficult to obtain an analytical solution for the BVP in (13) because it involves a nonlinear equation. However, we are only interested in the positive solution of (13) that has relevant biological meaning.

We rewrite IVP (13) as follows:

$$\begin{cases} \epsilon\phi_{1\rho\rho} + f(\rho)\phi_{1\rho} + g(\phi_1, \rho) = 0, \quad \rho \in (\eta, 1) \\ \epsilon\phi_{1\rho} - \phi_1 = 0, \quad \rho = \eta \text{ or } 1, \end{cases} \tag{14}$$

where

$$\epsilon = \frac{\delta_1}{\delta_2}, \quad f(\rho) = \frac{\epsilon}{\rho} - 1, \quad g(\phi_1, \rho) = -3\bar{a}\phi_1^3 - \frac{\phi_1}{\rho} + \frac{1}{\delta_2}, \quad \bar{a} = \frac{\delta_3(1-\delta_4)}{\delta_2}. \tag{15}$$

Note that ϵ is the ratio between diffusion and transport. Thus, $\epsilon \gg 1$ means the problem is diffusion-dominated, whereas $\epsilon \ll 1$ indicates that the problem is transport-dominated.

Next, we establish the existence of a positive solution for the IVP (14).

By making change to variables

$$\phi_1 = \exp\frac{\rho}{\epsilon}u(\rho) \tag{16}$$

Eq. (14) is written as

$$\begin{cases} \epsilon u_{\rho\rho} = F(\rho, u, u_\rho), \\ u_\rho = 0, \quad \rho = \eta \text{ or } 1, \end{cases} \tag{17}$$

where $F(\rho, u, u_\rho)$ is a continuous function, whose expression is given by

$$F(\rho, u, u_\rho) = -\left(\frac{1}{\delta_2}e^{-\rho/\epsilon} - 3\bar{a}e^{\frac{2\rho}{\epsilon}}u^3 + \left(1 + \frac{\epsilon}{\rho}\right)u_\rho\right). \tag{18}$$

For the above **Neumann** boundary value problem (17), the appropriate notions of lower and upper solutions are given as follows:

Definition 4.1. *A function $\alpha(\rho)$ is a lower solution of (17) that satisfies*

$$\epsilon\alpha_{\rho\rho} \geq F(\rho, \alpha, \alpha_\rho), \quad \alpha_\rho(\eta) \geq 0, \quad \alpha_\rho(1) \leq 0, \tag{19}$$

A function $\beta(\rho)$ is an upper solution of (17) that satisfies

$$\epsilon\beta_{\rho\rho} \leq F(\rho, \alpha, \alpha_\rho), \quad \beta_\rho(\eta) \leq 0, \quad \beta_\rho(1) \geq 0. \tag{20}$$

When $\alpha(\rho) \leq \beta(\rho)$, the **Neumann** boundary value problem (17) has a solution $u(\rho)$ such that for all $\rho \in [\eta, 1]$,

$$\alpha(\rho) \leq u(\rho) \leq \beta(\rho). \tag{21}$$

Theorem 4.2. *Consider the BVP (17). If $3\delta_3(1-\delta_4) < 1$ and $\epsilon < \frac{3\eta}{-\ln(3\delta_3(1-\delta_4))}$, then (17) has a positive solution.*

Proof. First, we consider the function $\beta(\rho) = 1$. By substituting $\beta(\rho)$ into (17), we obtain

$$-3\delta_3(1-\delta_4)e^{\frac{2\rho}{\epsilon}} + e^{-\frac{\rho}{\epsilon}} \tag{22}$$

When $3\delta_3(1-\delta_4) < 1$ and $\epsilon < \frac{3\eta}{-\ln(3\delta_3(1-\delta_4))}$, we have

$$-3\delta_3(1-\delta_4)e^{\frac{2\rho}{\epsilon}} + e^{-\frac{\rho}{\epsilon}} = e^{-\frac{\rho}{\epsilon}}\left(1 - 3\delta_3(1-\delta_4)e^{\frac{3\rho}{\epsilon}}\right) < 0. \tag{23}$$

Substituting $\beta(\rho)$ into the boundary condition in (17) yields

$$\beta_\rho = 0. \tag{24}$$

Thus, the function $\beta(\rho) = 1$ is an upper solution of (17).

Now, we let

$$\alpha(\rho) = e^{-\frac{1}{\epsilon}}(3\delta_3(1-\delta_4))^{-\frac{1}{3}}. \tag{25}$$

According to (23), we have

$$\alpha(\rho) \leq 1 = \beta(\rho). \tag{26}$$

By substituting $\alpha(\rho)$ into (17), we obtain

$$\frac{e^{-\frac{\rho}{\epsilon}} - e^{\frac{-3+2\rho}{\epsilon}}}{m} = \frac{e^{-\frac{\rho}{\epsilon}}(1 - e^{\frac{-3+3\rho}{\epsilon}})}{m} \geq 0. \tag{27}$$

It is easy to know that $\alpha(\rho)$ is a lower solution of Eq. (17). According to [21,22], the boundary value problem (17) has a bounded positive smooth solution $\phi(\rho)$ satisfying

$$0 < u(\rho) \leq 1, \quad \rho \in [\eta, 1], \tag{28}$$

which completes the proof.

According to (16), the solution $\phi_1(\rho)$ of Eq. (14) is satisfied

$$\exp\left(\frac{\eta}{\epsilon}\right)u(\rho) \leq \phi_1(\rho) \leq \exp\left(\frac{1}{\epsilon}\right)u(\rho) \tag{29}$$

As shown above, a steady-state solution for (14) exists for appropriate parameters. Specifically, $3\delta_3(1-\delta_4) = 3K_\alpha\frac{p_1^2}{(k_{13}+\gamma)^2}\frac{\gamma}{k_{13}+\gamma}$ holds, where the degradation parameter γ is very small and the equilibrium constant K_α is also small, according to [15]. Therefore, the condition $3\delta_3(1-\delta_4) < 1$ is readily satisfied. It is also clear that the condition $\epsilon < \frac{3\eta}{-\ln(3\delta_3(1-\delta_4))}$ plays an important role in determining the positive solution of (14).

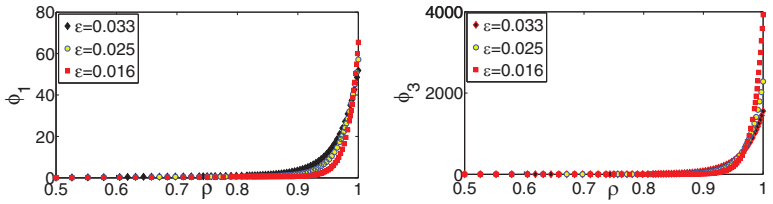

Fig. 4. The steady states ϕ_1 and ϕ_3 of (14) for $\delta_3 = 0.01$ and $\delta_4 = 0.998$ respectively.

The solution of the nonlinear BVP (14) cannot be obtained using an analytical method. If the parameter ϵ is small enough, this equation can be solved using the singular perturbation method. At the end point $\rho = 1$, there is a boundary layer for this problem and the asymptotic solutions are very complicated. Instead, we can find the steady state via numerical methods.

In Fig. 4, we plot the nondimensionalized ϕ_1 and ϕ_3 in the steady state for different parameters. Numerical experiments demonstrate that the parameter ϵ indeed plays a key role in determining Gag protein concentrations near the cell membrane. This figure shows that the monomeric and trimeric Gag proteins accumulate near the cell membrane and that the concentration of trimers is higher than that of monomers. In [19], the experimental data show that approximately 85% of the protein is in the trimeric state while 15% is in the monomeric state and that the proteins accumulate near the cell membrane. Therefore, our numerical results are in quantitatively good agreement with the experimental results.

5. Numerical simulations

In this section, we present numerical simulations for the model problem (4) to analyze the behaviors of the intracellular Gag protein monomers and trimers.

One important issue in the investigation of intracellular Gag protein movements is the time period when new HIV-1 virions first appear near the cell membrane. For convenience, we denote this time period as T_a. We present numerical simulations for the estimation of T_a and also examine the influence of the model parameters on T_a.

HIV-1 virions have a relatively wide range of diameters. In [20], it is shown that 95% of HIV-1 virions have diameters between 119 nm and 207 nm, corresponding to 3000 and 11, 000 Gag proteins, respectively. In this study, we assume that an average immature HIV-1 virion contains approximately 5000 copies of the Gag protein, as suggested in [20]. This implies that a threshold concentration of 4958 μM near the cell membrane is needed for new virions to appear.

5.1. Timing for New HIV-1 virions initial appearance on the plasma membrane

Model (4) is a nonlinear initial boundary value problem. Therefore, we apply a numerical method to analyze the model equations. The numerical scheme combines the standard finite difference (see [23]) with Newton–Raphson iterations. The discretization scheme is listed in Appendix A.

Table 1
The definitions and values of dimensionless parameters.

Processes	Parameters	Values
Equilibrium constant	K_α	0.005
Diffusion ratio	δ_1	0.006
Transport ratio	δ_2	0.0795
Association efficiency	δ_3	0.0221
Degradation efficiency	δ_4	0.99502

In Fig. 5, we plot the curves of ϕ_1 and ϕ_3 for three different locations (different ρ values in the cytoplasm). It is observed that the values of ϕ_1 and ϕ_3 for each ρ will reach a fixed constant after a short time period. Moreover, these values depend on ρ.

Using the same parameters, we plot the curves of ϕ_1 and ϕ_3 for $\rho = 1$ in Fig. 6. We observe that the values of ϕ_1 and ϕ_3 increase with respect to time. At the same time, the concentration of Gag proteins near the cell membrane is higher than that in the cytoplasm.

These results indicate that a boundary layer exists at $\rho = 1$ for the IBVP (4). In this case, the equilibrium constant is $K_\alpha = 0.005(\mu\text{M})^{-2}$, and the concentrations of f_1 and f_3 are 44.9605 and 4401.1, respectively. The Gag monomer concentration does not exceed 1.5%, whereas the Gag trimer concentration is at least 98.5%.

We now investigate the influence of the model parameters on T_a. Here, T_a is understood as the time period when the concentration of Gag proteins reaches the threshold value 4958 μM.

As mentioned in [16], Gag proteins accumulate and assemble at the plasma membrane. For simplicity, we consider only the nondimensional concentration of ϕ_1 and ϕ_3 near the end point $\rho = 1$. The corresponding concentrations of f_1 and f_3 near the cell membrane are $\frac{p_1}{k_{31}+\gamma}\phi_1$ and $\frac{p_1}{k_{31}+\gamma}\phi_3$, respectively.

We calculate T_a for different parameters and the values of parameters are listed Table 1. The results are plotted in Fig. 7. T_a increases with respect to parameters δ_1, δ_3, and K_α but decreases with respect to δ_2. These results indicate that fast diffusion, slow transport, and fast association all benefit the production of new virions.

5.2. Sensitivity analysis of model parameters

The sensitivity of T_a to a model parameter γ is defined as

$$S(\gamma) = \frac{T_a(\delta, \gamma + \Delta\gamma) - T_a(\delta, \gamma)}{T_a(\delta, \gamma)} \frac{\gamma}{\Delta\gamma}, \tag{30}$$

where γ and δ the disturbed and undisturbed parameters, respectively.

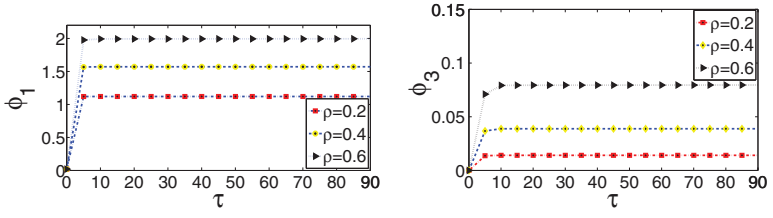

Fig. 5. Solutions of Eq. 4 for $\rho = 0.2, 0.4, 0.6$ and $\epsilon = 0.01$, $\delta_3 = 0.01$, $\delta_4 = 0.998$.

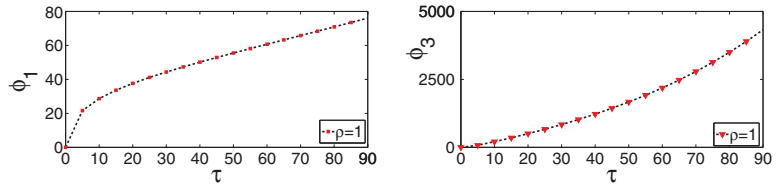

Fig. 6. Solutions of Eq. (4) for $\rho = 1$ and $\epsilon = 0.01, \delta_3 = 0.01, \delta_4 = 0.998$.

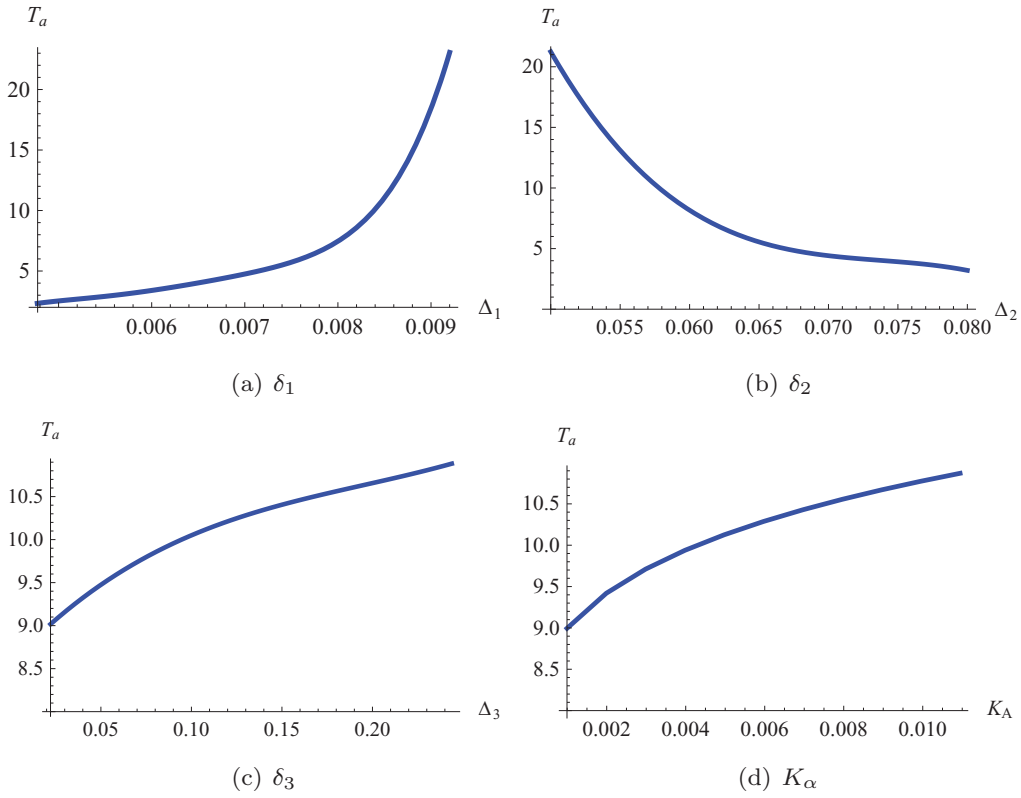

Fig. 7. Plots of time T_a(h) for different parameters. For subfigures (c) and (d), the values of parameters δ_1 and δ_2 are fixed at 0.0039801 and 0.012438, respectively.

In this section, we measure the sensitivity of T_a to parameters δ_1, δ_2 and δ_3 and the equilibrium constant K_α. The results are listed in Table 1. For these calculations, the values of $\Delta\delta_i (i = 1, 2, 3)$ are 10% of the corresponding parameters.

The results in Table 2 show that T_a is most sensitive to the diffusion ratio δ_1, and is also sensitive to the transport ratio δ_2, but it is not sensitive to the association efficiency δ_3. These results indicate that the perturbation of the diffusion and transport processes would greatly affect the timing when the first new virions appear near the cell membrane.

If we set the equilibrium constant to $K_\alpha = 0.005(\mu\text{M})^{-2}$ according to [15], we find that T_a is approximately 10.1 h based on the numerical simulations and Fig. 7(d). In [16], the experiment showed that the Gag protein assembly became detectable beginning at approximately 11 h post-transfection under some conditions, as demonstrated by Gag-Pol processing and extracellular particle release. The numerical results of the model equation are in good quantitatively agreement with the experiment results.

In this situation, the concentrations of f_1 and f_3 are 46.3421(μM) and 4950.12(μM), respectively. This indicates that most of the Gag proteins at the cell membrane remain in the trimeric state. In particular, at time $t = T_a$, the concentrations of Gag monomers and trimers near the cell membrane are 2% and 98%, respectively. These results demonstrate that our model is capable of reproducing the experimental data [19].

Table 2
Sensitivity of T_a to the model parameters.

$S(\delta)$	δ_1	δ_2	δ_3	K_α
S	13.293	3.9027	0.081	0.082

6. Concluding remarks

This paper presents a modeling study using differential equations to investigate the intracellular movement of HIV-1 Gag monomers and trimers. The monomers and trimers represent the two most important Gag protein species and play significant roles in the formation of HIV-1 immature virions. Our study is based on the assumptions that Gag monomers can diffuse in the cytoplasm and be transported by motor proteins along microtubules, whereas there is no diffusion or trafficking of Gag trimers. These assumptions are based on published biological studies and are used for modeling simplicity. Considering trafficking or diffusion of Gag trimers in a mathematical model will certainly provide more useful information about Gag protein intracellular movements. This topic is currently under investigation and will be reported in our future work. In addition, to verify the stability of HIV-1 Gag assembly, a stochastic model is expected in our next research [24].

This study focuses on the time period from the initial production of Gag protein monomers in the cytoplasm to the initial appearance

of immature HIV-1 virions near the cell membrane. Specifically, in our model, T_a is the time period when HIV-1 virions first appear near the cell membrane. For this time period, it is reasonable to impose zero total flux boundary conditions at both the inner and outer boundaries of the cytoplasm, which are represented by r_a and r_b, respectively, in our model. After time T_a, Gag multimerization will still occur near the cell membrane, but this occurs simultaneously with the budding of HIV-1 virions from the cell membrane. For this time period, a "leaking" boundary condition should be imposed at r_b (the cell membrane). Solving boundary value problems with a "leaking" boundary condition is a mathematically interesting research topic and will also contribute to a better understanding of the HIV-1 budding process.

Acknowledgments

The authors thank the anonymous reviewers for their helpful comments and suggestions. The work of the first, second, and fifth authors was partially supported by the Major Research Plan of the National Natural Science Foundation of China, China (no. 91230118) and the National Natural Science Foundation of China, China (no. 61173060). The third author was partially supported by the US National Science Foundation under grant EAPSI-1415117.

Appendix A. Discretization of the model equations

First, we discrete the model equations by the Crank–Nicolson method. For simplicity, let $\phi_{1n}^k = \phi_1(n\Delta\rho, k\Delta\tau)$ and $\phi_{3n}^k = \phi_3(n\Delta\rho, k\Delta\tau)$. The derivatives of ϕ_1 with respect to τ and ρ are respectively discretized as follows

$$\begin{cases} \dfrac{\partial\phi_1}{\partial\tau} = \dfrac{\phi_{1n}^{k+1} - \phi_{1n}^k}{\Delta\tau}, \\ \dfrac{\partial^2\phi_1}{\partial\rho^2} = \dfrac{1}{2(\Delta\rho)^2}\left(\left(\phi_{1(n+1)}^{k+1} - 2\phi_{1n}^{k+1} + \phi_{1(n-1)}^{k+1}\right)\right. \\ \left. + \left(\phi_{1(n+1)}^{k} - 2\phi_{1n}^{k} + \phi_{1(n-1)}^{k}\right)\right), \\ \dfrac{\partial\phi_1}{\partial\rho} = \dfrac{1}{2}\left(\dfrac{\phi_{1(n+1)}^{k+1} - \phi_{1(n-1)}^{k+1}}{2\Delta\rho} + \dfrac{\phi_{1(n+1)}^{k} - \phi_{1(n-1)}^{k}}{2\Delta\rho}\right). \end{cases} \tag{A.1}$$

From the second equation in (4), we have

$$\phi_{3n}^k = K_1\phi_{3n}^{k-1} + K_2(\phi_{1n}^k)^3. \tag{A.2}$$

Then (4) is discretized as follows

$$\begin{aligned} &A_n(\phi_{1n}^k)^3 + B_n\phi_{1n}^k + C_n\phi_{1(n+1)}^k + D_n\phi_{1(n-1)}^k \\ &\quad = E_n\phi_{1n}^{k-1} + F_n\phi_{1(n+1)}^{k-1} + G_n\phi_{1(n-1)}^{k-1} + H_n, \\ &\quad n = 1, 2, \ldots, N-1, \end{aligned} \tag{A.3}$$

where

$$\begin{aligned} &A_n = 3\delta_3\Delta\tau - 3\delta_3K_2\Delta\tau, \quad B_n = 1 + \frac{\delta_1\Delta\tau}{(\Delta\rho)^2} + \frac{\delta_2\Delta\tau}{n\Delta\rho}, \\ &C_n = -\frac{\delta_1\Delta\tau}{2(\Delta\rho)^2} - \frac{k_n\Delta\tau}{4\Delta\rho}, \quad D_n = -\frac{\delta_1\Delta\tau}{2(\Delta\rho)^2} + \frac{k_n\Delta\tau}{4\Delta\rho}, \\ &E_n = 1 - \frac{\delta_1\Delta\tau}{(\Delta\rho)^2}, \quad F_n = \frac{\delta_1\Delta\tau}{2(\Delta\rho)^2} + \frac{k_n\Delta\tau}{4\Delta\rho}, \\ &G_n = \frac{\delta_1\Delta\tau}{2(\Delta\rho)^2} - \frac{k_n\Delta\tau}{4\Delta\rho}, \quad H_n = 3\delta_4\phi_{3n}^{k-1}\Delta\tau K_1 + \Delta\tau, \\ &K_1 = \frac{1}{1+\Delta\tau}, \quad K_2 = \frac{\Delta\tau\delta_3}{1+\Delta\tau}, \quad k_n = \frac{\delta_1}{n\Delta\rho} - \delta_2. \end{aligned} \tag{A.4}$$

Applying the boundary conditions leads to

$$\begin{cases} A_0(\phi_{10}^k)^3 + \phi_{10}^k(B_0 - 2D_0\delta_{21}\Delta\rho) + \phi_{11}^k(C_0 + D_0) \\ = (E_0 - 2G_0\delta_{21}\Delta\rho)\phi_{10}^{k-1} + \phi_{11}^{k-1}(F_0 + G_0) + H_0, \\ A_N(\phi_{1N}^k)^3 + \phi_{1N}^k(B_N + C_N2\delta_{21}\Delta\rho) + \phi_{1(N-1)}^k(D_N + C_N) \\ = \phi_{1N}^{k-1}(E_N + 2F_N\delta_{21}\Delta\rho) + \phi_{1(N-1)}^{k-1}(G_N + F_N) + H_N. \end{cases} \tag{A.5}$$

The systems (A.3) and (A.5) have $N+1$ unknowns $\phi_{10}^k, \ldots, \phi_{1N}^k$ and are rewritten using vectors as

$$\mathbf{Q}(\mathbf{X}^k)\mathbf{X}^k = \mathbf{P}\mathbf{X}^{k-1}, \tag{A.6}$$

where $\mathbf{X}^k = (\phi_{10}^k, \phi_{11}^k, \ldots, \phi_{1N}^k)^{\mathrm{T}}$ is the unknown vector and $\mathbf{Q}, \mathbf{P}$ are $(N+1)\times(N+1)$ matrices, which depend on B_n, C_n, D_n, X^k and E_n, F_n, G_n, H_n, respectively.

At each time step $\tau_k = k\Delta\tau$, Eq. (A.6) is a nonlinear algebraic equation, which is solved by the Newton–Raphson iterative method as follows

$$\begin{cases} n = 0, 1, 2, \ldots, \quad \mathbf{X}_0^k = \mathbf{X}^{k-1}, \\ \mathbf{J}_n = \left(\dfrac{\partial\mathbf{Q}(\mathbf{X}^k)(\mathbf{X}^k)}{\partial\mathbf{X}^k}\right)^{-1}|_{\mathbf{X}^k=\mathbf{X}_n^k}, \\ \Delta\mathbf{X}_n^k = -\mathbf{J}_n\left(\mathbf{Q}(\mathbf{X}_n^k)(\mathbf{X}_n^k) - \mathbf{P}\mathbf{X}^{k-1}\right), \\ \mathbf{X}_{n+1}^k = \mathbf{X}_n^k + \Delta\mathbf{X}_n^k \end{cases} \tag{A.7}$$

It is shown that $\mathbf{X}_n^k$ converges to $\mathbf{X}^k$.

References

[1] W. Sundquist, H. Hrausslich, HIV-1 assembly, budding, and maturation, Cold Spring Harbor Perspect. Med. 2 (2012) a006924.
[2] Y. Morikawa, HIV capsid assembly, Curr. HIV Res. 1 (2003) 1–14.
[3] S. Jin, Y. Li, R. Pan, X. Zou, Characterizing and controlling the inflammatory network during influenza A virus infection, Sci. Rep. 4 (2014) 3799.
[4] J. Tan, R. Pan, L. Qiao, X. Zou, Z. Pan, Modeling and dynamical analysis of virus-triggered innate immune signaling pathways, PLoS One 7 (2012) e48114.
[5] W. Zhang, X. Zou, Systematic analysis of the mechanisms of virus-triggered type I IFN signaling pathways through mathematical modeling, IEEE/ACM Trans. Comput. Biol. 10 (2013) 771–779.
[6] M. Muller, S. Klumpp, R. Lipowsky, Tug-of-war as a cooperative mechanism for bidirectional cargo transport by molecular motors, Proc. Natl. Acad. Sci. U.S.A. 25 (2008) 4609–4614.
[7] A. Kunwar, S. Tripathy, J. Xu, M. Mattson, P. Anand, R. Sigua, M. Vershinin, R. McKenney, C. Yu, A. Mogilner, S. Gross, Mechanical stochastic tug-of-war models cannot explain bidirectional lipid-droplet transport, Proc. Natl. Acad. Sci. U.S.A. 22 (2011) 18960–18965.
[8] A. Dinh, D. Pangarkar, T. Theofanous, S. Mitragotri, Understanding intracellular transport processes pertinent to synthetic gene deliver via stochastic simulations and sensitivity analysis, Biophys. J. 92 (2007) 831–846.
[9] T. Lagache, D. Holcman, Effective motion of virus trafficking inside a biological cell, SIAM J. Appl. Math. 68 (2008) 1146–1167.
[10] A. Dinh, T. Theofanous, S. Mitragotri, A model for intracellular trafficking of adenoviral vectors, Biophys. J. 89 (2005) 1574–1588.
[11] A. Kuznetsov, A. Avramenko, Analytical investigation of transient molecular-motor-assisted transport in elongated cells, Cent. Eur. J. Phys. 6 (2008) 45–51.
[12] J. Liu, R. Munoz-Alicea, T. Huang, S. Tavener, C. Chen, A mathematical model for intracellular HIV-1 Gag protein transport and its parallel numerical simulations, Procedia Comput. Sci. 9 (2012) 679–688.
[13] M. Resh, A myristoyl switch regulates membrane binding of HIV-1 Gag, Proc. Natl. Acad. Sci. U.S.A. 13 (2004) 417–418.
[14] J. Tan, X. Zou, Complex dynamical analysis of a coupled system from innate immune responses, Int. J. Bifurcation Chaos 23 (2013) 1350180.
[15] C. Tang, E. Loeliger, P. Luncsford, I. Kinde, D. Beckett, M. Summers, Entropic switch regulates myristate exposure in the HIV-1 matrix protein, Proc. Natl. Acad. Sci. U.S.A. 13 (2004) 511–517.
[16] N. Jouvenet, S. Neil, C. Bess, M. Johnson, C. Virgen, S. Simon, P. Bieniasz, Plasma membrane is the site of productive HIV-1 particle assembly, PLoS Biol. 4 (2006) 2296–2310.
[17] C.S. Adamson, E.O. Freed, Human immunodeficiency virus type 1 assembly, release, and maturation, Adv. Pharmacol. 55 (2007) 347–387.
[18] A. Ona, Relationships between plasma membrane microdomains and HIV-1 assembly, Biol. Cell 102 (2010) 335–350.
[19] S. Datta, Z. Zhao, P. Clark, Interactions between HIV-1 Gag molecules in solutions: an inositol phosphate-mediated switch, J. Mol. Biol. 19 (2007) 799–811.
[20] J. Briggs, M. Simon, The stoichiometry of Gag protein in HIV-1, Nat. Struct. Mol. Biol. 11 (2004) 672–675.

[21] C. De Coster, P. Habets, An overview of the method of lower and upper solutions for ODEs, in Nonlinear Analysis and its Applications to Differential Equations. vol. 43: Progress in Nonlinear Differential Equations and Their Applications, pp. 3–22, Birkhauser, Boston, Mass, USA, 2001.
[22] A. Cabada, An overview of the lower and upper solutions method with nonlinear boundary value conditions, Bound. Value. Probl, (2011), doi:10.115/2011/893753.
[23] J. Strikwerda, Finite Difference Schemes and Partial Differential Equations, Wadsworth Brooks/Cole, Pacific, CA, 1990.
[24] Y. Li, M. Yi, X. Zou, The linear interplay of intrinsic and extrinsic noises ensures a high accuracy of cell fate selection in budding yeast, Scientific Reports, 4 (2014), 5764.